Research Article

Minjie Zhang*, Yanqiu Yu, Jinyong Choi, Kui Cai, and Mingyuan Shi

Petrography and geochemistry of clastic sedimentary rocks as evidence for the provenance of the Jurassic stratum in the Daqingshan area

https://doi.org/10.1515/geo-2020-0146
received May 20, 2020; accepted October 13, 2020

Abstract: The Daqingshan area is located in the Khondalite belt in the northern margin of the North China Craton. It has the best-preserved Mesozoic basin and is an ideal area for research on Jurassic strata. Sandstones mainly contain quartz and feldspar, with significantly less debris content. In addition, petrography and geochemical classifications have revealed the presence of arkose and wacke. Chondrite-normalized rare earth element patterns of samples are characterized by the enrichment of light rare elements and the flat trend toward heavy rare earth elements. Petrography and source rock discrimination diagrams of geochemical data suggest the presence of felsic rock and Precambrian basement in the northern and southern parts of the basin, which are crucial source areas; however, few mafic materials occur in the Wudanggou Formation. Tectonic discrimination diagrams of geochemical data show that the source materials were deposited on an active continental margin and/or continental island arc. Petrological and geochemical data from the Wudanggou Formation and Changhangou Formation samples suggest that the Yanshan movement influenced the formation of the Changhangou Formation.

Keywords: Khondalite belt, Daqingshan area, Jurassic strata, geochemical, provenance, tectonic setting

*** Corresponding author: Minjie Zhang,** Hebei Key Laboratory of Strategic Critical Mineral Resources, Hebei GEO University, Shijiazhuang 050031, China; Department of Oceanography, Kunsan National University, Gunsan 573-701, Republic of Korea, e-mail: mj-zhang@hgu.edu.cn
Yanqiu Yu: Hebei Key Laboratory of Strategic Critical Mineral Resources, Hebei GEO University, Shijiazhuang 050031, China
Jinyong Choi: Department of Oceanography, Kunsan National University, Gunsan 573-701, Republic of Korea
Kui Cai: Institute of Geological Survey, Hebei GEO University, Shijiazhuang 050031, China
Mingyuan Shi: The Sixth Geological Exploration Division, Hebei Bureau of Geological Exploration and Development, Shijiazhuang 050085, China

1 Introduction

Sedimentary rocks are the only evidence of the ancient upper crust that might have been removed by erosion, covered by sedimentary deposits or ice, or buried deep in the crust. The combination of detrital and geochemical compositions of sedimentary rocks provides important information on the characteristics of their provenance and tectonic setting [1,2]. The basin received sediments from surrounding orogenic belts, preserving evidence of orogenic belt elevation, thus reflecting the history of orogenic belt erosion [3,4]. Therefore, the study of basins should be closely linked to that of the orogenic belts.

The North China Craton (NCC) is one of the oldest continental blocks in the world. The Daqingshan area is part of the north margin of NCC located in the Khondalite belt (see Figure 1a). It primarily comprises the northern Jurassic basin and the southern Daqingshan fold and thrust system (see Figure 1b). In the last decade, the Yinshan area has been extensively investigated in terms of thrust nappe system [5–9] and lithology [10,11], geochemistry [12–14], and geochronology [15–30] of the Precambrian basement.

The northern margin of the NCC has a complex history of tectonic evolution since the Mesozoic time [5,9]. A large-scale thrust nappe developed in the Daqingshan area during the Indosinian–Yanshanian epoch [5,9]. An Indosinian thrust nappe that formed in the Late Triassic–Early Jurassic caused the crust to undergo strong compression and later tension, thereby forming the Jurassic Basin [31,32]. The time of origin of the Daqingshan nappe in Yanshanian is uncertain. Some researchers suggest that the thrust nappe formed during 125–121 Ma [31], whereas others believe that the thrust nappe formed toward the end of the Middle Jurassic [33,34]. Recently, several researchers have agreed that the age range of 125–121 Ma is correct for the late Yanshanian nappe, starting before 160 Ma [35–38].

The Jurassic basin of the Daqingshan area is the most well-preserved Mesozoic basin in the Yinshan area, which is the ideal area for exploring the Jurassic strata. The geochemistry and tectonic setting of the Jurassic strata have

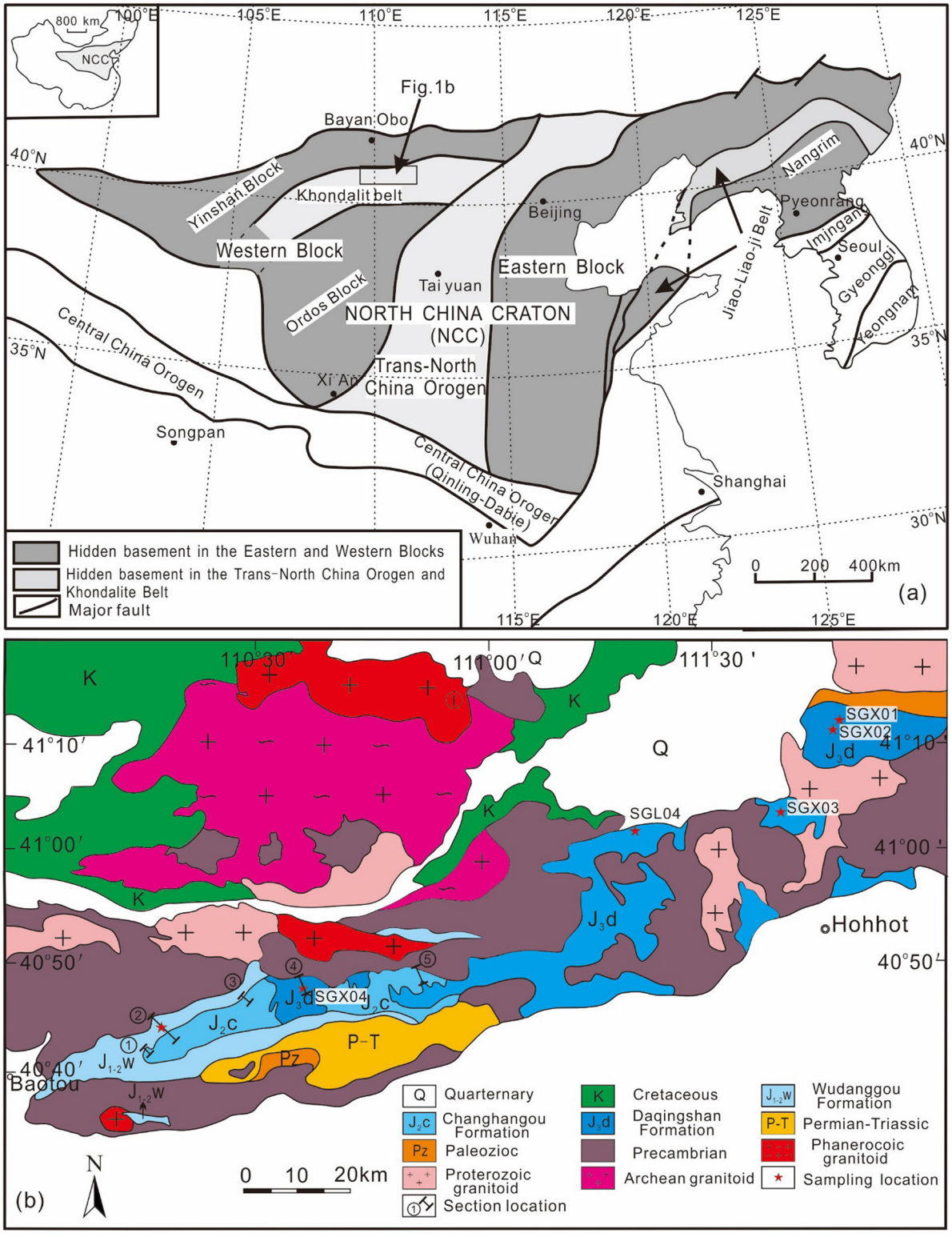

Figure 1: (a) Location of Daqingshan area in the North China Craton (modified from ref. [39]). (b) Geological map of the study area (modified from ref. [40]).

not been studied in detail. The purpose of this study is to evaluate sandstone petrography and the major and trace elemental geochemistry of the Jurassic strata to understand their provenance, tectonic setting, and weathering condition during Jurassic; the resulting findings will be useful in reconstructing the palaeogeography of the region.

2 Geological setting

The Precambrian basement in the Daqingshan area primarily contains gneiss, granulite, and granite. Cambrian and Ordovician strata unconformably overlie basement rocks in confined areas and mainly comprise erosion-resistant carbonate and minor sandstone, shale, and local pebbly conglomerate along the unconformity [41]. Permian and Triassic terrigenous clastic rocks are found south of the basin, and they mainly include purplish-red fluvial siltstone, sandstone, and conglomerate together with minor syenite (233 ± 7 Ma) that intruded the basement near the present-day site of Yongfu Village [42].

The Early–Middle Jurassic strata (Wudanggou Formation) in the basin were controlled through synchronous normal faulting [31,41]. The Wudanggou Formation exhibits an unconformable contact with the Precambrian basement. The Wudanggou Formation mainly crops out in the western part of the basin (see Figure 1b), with several more E–W erosional remnants in the southwest of the Daqingshan range [37]. The lower section of the Wudanggou Formation primarily comprises cobble-boulder conglomerate with a few decimeters to more than 2 m, indicating fan deltaic facies. The middle section is mainly an interbedding of pebbly sandstones and gritrocks. Sandstone beds are typically marked by erosive bases and trough or cross-beddings (see Figure 2b). These changes suggest a braided river system in the middle Wudanggou Formation, and the upper Wudanggou Formation dominated by sandstones with interbedded silty mudstones shows a shallow-lacustrine system (see Figure 2). According to regional stratigraphic correlation and radiometric age controls [31,43–45], the lower part of the Wudanggou Formation is equivalent to the Xingshikou Formation (198 ± 5 Ma) in the Yanshan belt [46], and the upper part is equivalent to the combined Yondingzhuang and Datong formations (179–171 Ma) in the Taihang Mountains [44,47]. The flora assemblage in the Upper Wudanggou Formation indicates that the formation is Early–Middle Jurassic in age [48].

The Middle Jurassic Changhangou Formation is distributed in the middle of the basin. The lower beds are characterized by thick-bedded to massive, coarse-grained sandstone (see Figure 2). Consequently, the sandstone-dominated sequence is interpreted to have been a braided river system [37]. Both grain size and bed thickness of the sandstone decrease upward, and the siltstone and mudstone portions represent shallow and deep parts of a lacustrine system. The upper section mainly comprises medium- to coarse-grained sandstone, with variable large-scale cross-stratifications intercalated with minor thin-bedded siltstone, representing a shore-shallow-lacustrine system indicative of lake water and mass recession (see Figure 2). Zircon U–Pb dating of the volcanic materials from the Changhangou Formation yields an age of 163.7 ± 1.0 Ma [37], suggesting that the Changhangou Formation is Middle Jurassic in age. This may indicate a relationship between the deposition of the Changhangou Formation and the initiation of the Yanshanian nappe in the Daqingshan area.

The Daqingshan Formation has a disconformable contact with the underlying Changhangou Formation [33]. The lower member of the section mainly includes unsorted, clast-supported, cobble–pebble conglomerate, intercalated with minor coarse-grained or pebbly sandstone, representing a proximal alluvial environment. The proportion of siltstone and sandstone gradually increases in the upper part of the Daqingshan Formation, indicating a relatively distal fluvial system (see Figure 2). Regionally, the Daqingshan Formation correlates well with the Tuchengzi Formation in the Yanshan belt. Previous researchers suggested that the geologic age of the Tuchengzi Formation should be 154–137 Ma [49–51].

3 Methods

Sandstone and mudstone samples were collected from Baicaigou town and Wuchuan city. Twenty-one thin sections of sandstone were used for modal analysis. We performed a modal analysis of the delegate sandstones through the Gazzi Dickinson method using more than 300 points per sample. According to this method, monocrystalline quartz (Qm), polycrystalline quartz (Qp), plagioclase (Pl), K-feldspar (Kf), lithic fragments (L), and mica (M) were counted. Petrofacies were classified based on Folk's [52]. Samples were selected for geochemical analysis: 10 siltstone or mudstone samples and 9 sandstone samples. All geochemically analyzed samples from the Wudanggou Formation and Changhangou Formation are from the Baicaigou section (see Figure 3). Geochemically analyzed samples from the Daqingshan Formation were scattered according to outcrop distribution (Figure 1b).

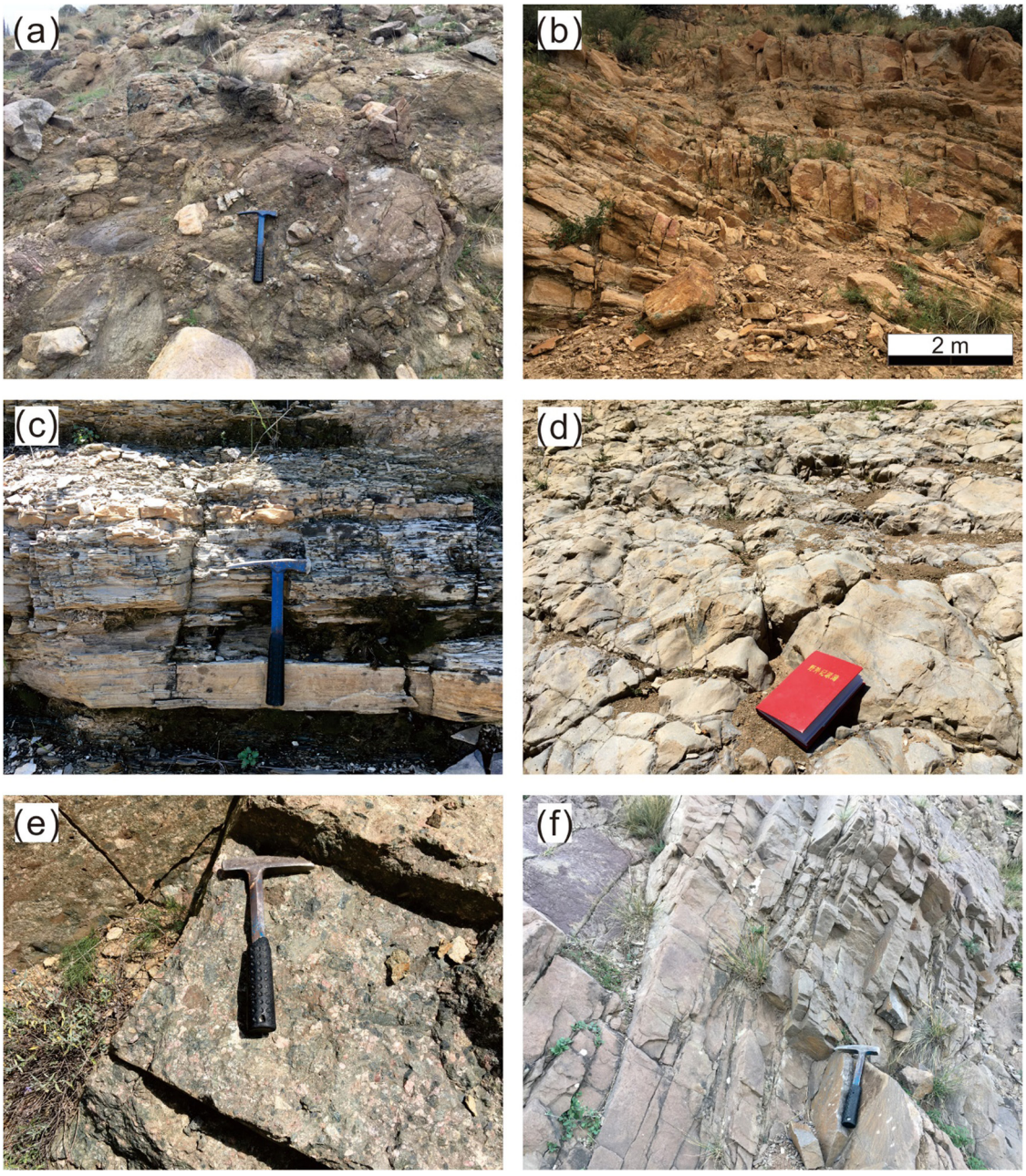

Figure 2: Field photographs of the Jurassic strata in Daqingshan area; (a) cobble-bould conglomerate in lower Wudanggou Formation. (b) Sandstone beds with cross-beddings. (c) Horizontal bedding occurs in Changhangou Formation. (d) A weathering-denuding surface in upper Changhangou Formation. (e) Polymictic conglomerates in lower Daqingshan Formation. (f) Thick middle sandstone in Daqingshan Formation.

Bulk chemical analyses of major, trace, and rare earth elements (REEs) were performed at the Hebei Province Regional Geology Institute. Major element analysis was performed using a Phillips PW 1480 X-ray fluorescence spectrometer (XRF). Total Fe was reported as Fe_2O_3. Loss on ignition (LOI) was measured by weighing before and after 1 h ignition at 1,000°C. Trace elements and REEs were determined via inductively coupled plasma-mass spectrometry (ICP-MS). The accuracy of the XRF analyses was estimated to be better than 1%. Analytical precision for trace elements and the REEs is generally better than 5%.

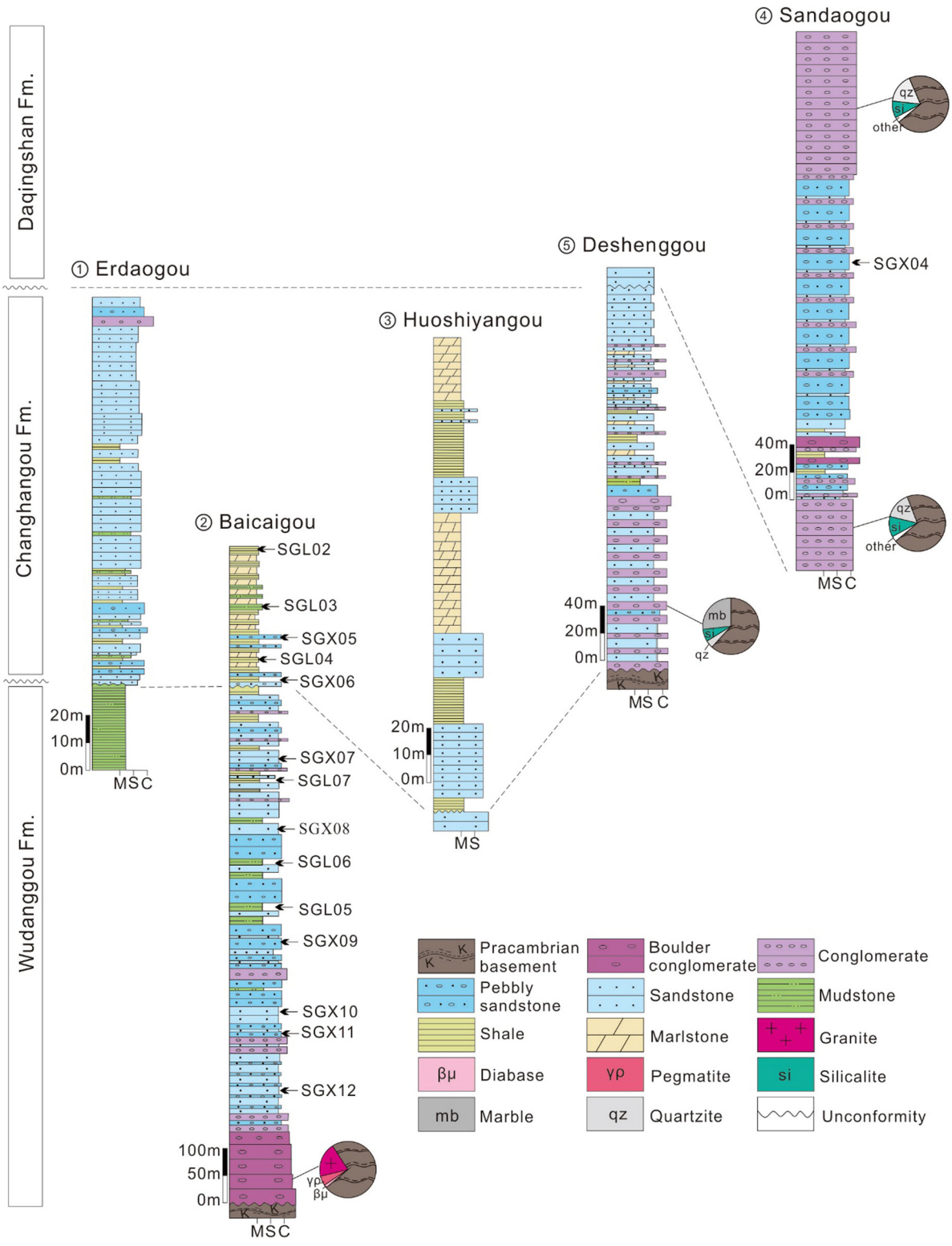

Figure 3: Measured stratigraphic sections from west to east: Erdaogou, Baicaigou, Houshiyangou, Sandaogou, and Deshenggou. See Figure 1b for sections location. C: conglomerate; S: sandstone; M: mudstone.

4 Results

4.1 Petrography

Petrographic analyses of sandstones were performed to determine the sandstone as well as the tectonic and sedimentary histories [54]. Petrographic composition and detrital modes of the Jurassic sandstones are presented in Table 1.

The sandstones of the Wudanggou Formation comprise subrounded to angular, moderately sorted, immature, medium to coarse sandstones (see Figure 4a and b). Partial sericitization of plagioclase can be observed in sample SGX08 (see Figure 4b). The quartz grains are Qm and Qp, ranging from 35% to 52% and 6% to 15%, respectively (see Table 1). Feldspar is mainly plagioclase (18–39%), whereas K-feldspar occurs in minor amounts ranging from 2 to 18% (see Table 1). Compared with the Wudanggou Formation, the sandstone from the Changhangou Formation contains more feldspar (61–67%) and less quartz (29–36%). The quartz grains are mostly Qm, and Feldspar is mainly plagioclase. The sandstone from the Changhangou Formation primarily contains plagioclase (53–64%) and quartz (32–43%). Additionally, more mica is present in the sandstones from the Daqingshan Formation, ranging from 1 to 8% (see Figure 4c).

To classify the studied sandstones according to the Folk classification [53], quartz (Q), feldspar (F), and total unstable rock fragment (Lt) were recalculated to 100% ignoring the cements, matrix, and accessory minerals (see Table 1). The studied sandstones mainly fall within the arkose fields (see Figure 5).

Table 1: Modal analysis data of Jurassic sandstones in the Daqingshan area

Sample	Qm	Qp	Pl	Kfs	L	M	QFLt (%)		
							Q	F	Lt
Daqingshan Formation									
SGX01	35	4	53	1	1	6	42	57	1
SGX02	29	2	59	1	1	8	34	65	1
SGX03	38	2	55	2	1	2	41	58	1
P22B 2-1	30	2	59	1	3	5	34	63	3
P22B 5-1	31	1	62	2	2	2	33	65	2
P22B 6-4	29	2	58	2	1	8	34	65	1
P22B 10-1	30	2	64	1	2	1	32	66	2
Changhanhou Formation									
P23B 1-1	28	1	65	2	1	3	29	69	2
P23B 2-2	34	2	60	1	3	1	35	61	4
Wudanggou Formation									
SGX07	52	6	38	3	1	0	58	41	1
SGX08	48	6	37	8	1	0	54	45	1
SGX09	50	13	18	18	1	0	63	36	1
SGX10	52	8	35	4	1	0	60	39	1
SGX11	39	15	36	6	0	1	54	44	2
SGX12	54	7	32	2	1	2	64	35	1
P18B 5-1	46	7	38	7	2	0	53	45	2
P18B 6-1	44	9	35	11	1	0	53	46	1
P18B 7	49	13	30	7	1	0	60	37	3
P18B 7-3	40	9	35	14	1	1	49	49	1
P18B 7-7	42	8	39	10	1	0	50	49	1
P18B 9-2	35	10	35	18	1	1	45	54	1

Qm = monocrystalline quartz grains; Qp = polycrystalline quartz grains; Pl = plagioclase; Kfs = K-feldspar; L = lithic fragments; M = mica; Q = Qm + Qp; F = Pl + Kfs; Lt = total unstable rock fragments.

5 Geochemistry

5.1 Major elements

Table 2 lists the major element data that reflect the mineralogy of the studied samples. SiO_2 content and the K_2O/Na_2O ratio in samples from the Wudanggou Formation are greater than those from the Changhangou Formation and Daqingshan Formation.

The SiO_2/Al_2O_3 ratio reflects the abundance of quartz as well as clay and feldspar content, and the Na_2O/K_2O ratio is an index of chemical maturity [55]; however, the Fe_2O_3/K_2O ratio enables better classification of arkoses and measured mineral stability [56]. The geochemical classification diagram revealed the samples from the Daqingshan Formation to be wackes (see Figure 6). The samples SGX05 and SGX06 from the Changhangou Formation are shales and/or mudstones, whereas other samples are wackes. The samples from the Wudanggou Formation are mainly arkose (see Figure 6). This suggests that the Jurassic sandstones were formed by rapid erosion, transport, and deposition.

5.2 Trace elements

Trace elements (particularly inactive ones) in rocks are usually well retained in the sediment during weathering and transportation; thus, the composition and content of trace elements in the sediments provide an effective way to trace the characteristics and structural features of the source rock [57,58].

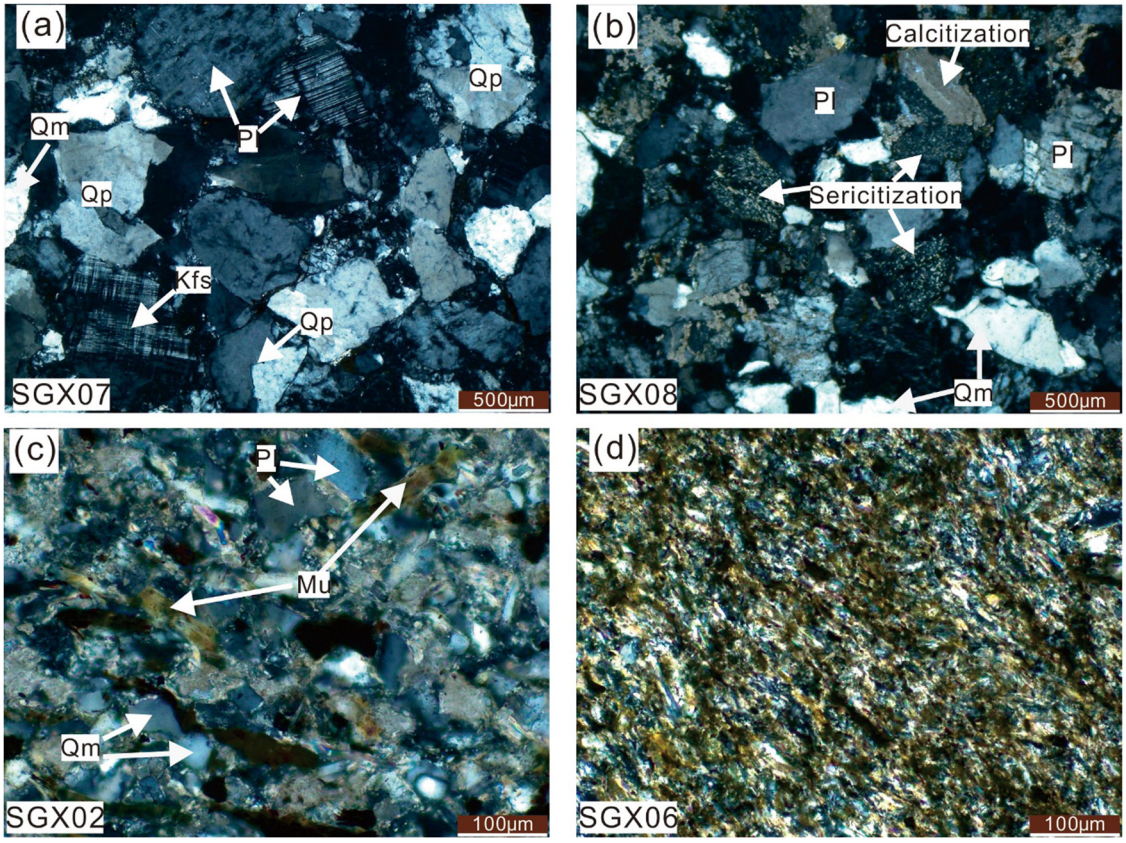

Figure 4: Representative thin-section of the Jurassic clastic rocks under cross-polarized; (a) polycrystalline quartz and K-feldspar grains in the sandstone of Wudanggou Formation. (b) Plagiocalase grains with calcitization or sercitization in the sandstone of Wudanggou Formation. (c) Mica grains in the sandstone of Daqingshan Formation. (d) Mudstone with weakly metamorphoic from Changhangou Formation. Qm = monocrystalline quartz grains; Qp = polycrystalline quartz grains; Pl = plagioclase; Kfs = K-feldspar; Mu = muscovite.

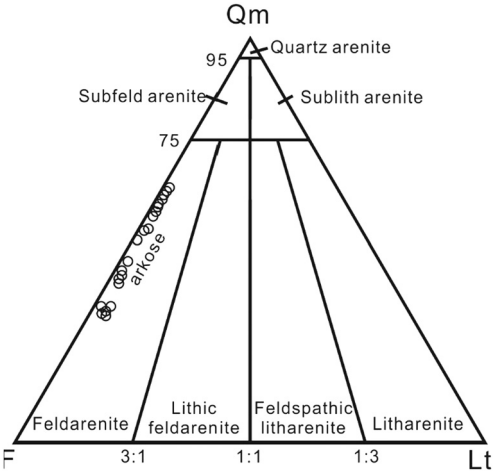

Figure 5: Classification diagram of the studied sandstones (fields after ref. [53]).

A comparison of these Jurassic sediments with the average upper continental crust (UCC) [59] reveals that the concentration of the samples is lower except for Ni, Cr, and V in samples with the primitive mantle-normalized patterns (see Figure 7) [60]. Distribution curves of UUC and the samples are similar, indicating that the source is upper crust rocks.

5.3 Rare earth elements

Trace and REE composition of samples are listed in Table 2. The REE content in our samples ranged from 102.16 to 355.16 ppm with an average of 164.93 ppm, which is less than the range for Post-Archean Australian Shale (PAAS) [61] but greater than that of UCC [59]. The ratios of light rare earth elements (LREEs)/heavy rare earth elements (HREEs) and (La/Yb)n are 7.51–24.12 and 7.42–35.87, respectively.

In the PAAS – normalized plot, the samples from the Wudanggou Formation show a gentle pattern with pronounced positive Eu anomalies in contrast with those of the samples from the Changhangou Formation and

Table 2: Major element concentrations (wt%) of Jurassic strata in the Daqingshan area

Layer	Samples	SiO_2	Al_2O_3	Fe_2O_3	FeO	MgO	CaO	Na_2O	K_2O	TiO_2	P_2O_5	MnO	LOI	Total	CIA	ICV
Daqingshan Formation	SGX01	61.73	13.15	2.71	2.07	3.27	4.44	2.36	2.73	0.62	0.21	0.06	6.38	99.73	63.80	1.23
	SGX02	60.05	13.47	3.27	2.19	3.78	4.47	2.19	2.92	0.70	0.21	0.07	6.48	99.80	64.90	1.29
	SGX03	64.17	13.59	4.14	0.40	3.45	3.28	3.12	2.81	0.61	0.19	0.06	4.01	99.83	61.30	1.28
	SGX04	63.59	17.15	4.19	1.15	2.43	0.48	0.26	4.39	0.54	0.08	0.13	5.42	99.81	77.90	0.72
	SGL01	65.36	14.95	3.38	1.06	2.46	2.46	1.82	2.60	0.62	0.83	0.07	4.13	99.75	68.50	0.89
Changhangou Formation	SGX05	11.81	2.76	0.44	2.52	5.84	37.88	0.51	0.58	0.12	0.77	0.47	36.11	99.81	63.30	0.81
	SGX06	51.57	18.61	8.43	0.60	2.95	1.67	4.15	2.83	1.09	0.13	0.03	7.76	99.82	69.40	1.13
	SGL02	64.94	16.55	3.202	0.98	1.86	1.76	1.13	2.78	0.62	0.11	0.04	5.61	99.58	76.70	0.75
	SGL03	53.44	15.68	5.12	1.69	2.65	6.02	0.71	3.28	0.58	0.13	0.16	10.16	99.62	77.50	1.29
	SGL04	58.98	17.61	3.74	2.56	2.56	4.84	1.55	2.01	0.25	0.27	0.04	5.07	99.48	77.50	1.01
Wudanggou Formation	SGX07	77.65	12.68	0.63	0.20	0.08	0.32	1.55	3.31	0.77	0.10	0.01	2.46	99.76	71.00	0.53
	SGX08	72.94	11.31	0.79	1.07	0.38	3.30	1.59	3.75	0.24	0.05	0.05	4.29	99.76	62.00	0.89
	SGX09	76.84	11.56	2.21	0.48	0.16	0.36	1.84	3.15	0.55	0.12	0.05	2.37	99.69	68.40	0.72
	SGX10	78.79	10.16	0.89	0.05	0.07	1.62	1.61	3.70	0.14	0.05	0.09	2.6	99.77	60.00	0.79
	SGX11	73.52	11.81	4.84	0.16	0.16	0.59	0.87	3.72	0.47	0.09	0.06	3.45	99.74	70.80	0.90
	SGX12	69.07	13.08	3.73	0.80	0.20	2.31	0.54	3.52	0.61	0.02	0.06	5.79	99.73	74.00	0.83
	SGL05	74.03	12.60	3.26	0.604	0.48	1.26	1.53	3.13	0.46	0.09	0.06	2.36	99.86	69.20	0.80
	SGL06	71.81	14.04	2.66	1.274	0.95	1.19	1.02	3.24	0.51	0.11	0.10	2.87	99.77	73.40	0.68
	SGL07	72.93	12.06	2.79	0.991	0.69	1.19	1.66	3.32	0.45	0.08	0.04	3.59	99.79	67.10	0.84

Daqianshan Formation (see Figure 8b, d and f). The chondrite-normalized pattern of the samples shows high LREEs (see Figure 8a, c and e). Samples from the Wudanggou Formation show pronounced positive Eu anomalies (δEu = 1.23), whereas the samples from the Changhangou Formation show more pronounced negative Eu anomalies (δEu = 0.67) than the Daqingshan Formation samples (δEu = 0.86) (see Table 3). Eu is mainly enriched in plagioclase during magma differentiation but is relatively incompatible with other minerals [62]. The δEu value indicated that the source rock of the Changhangou Formation and Daqingshan Formation generally tends toward granitic. Rocks and source rocks of the Wudanggou Formation may be mixed with mafic components.

δCe values can reflect the redox environment of sediments. Ce mainly exists as Ce^{3+} in the sediments; however, it is precipitated as Ce^{4+} in an oxidizing depositional environment, which is a negative δCe anomaly [62]. The δCe values of the Wudanggou Formation and Changhangou Formation ranged from 0.86 to 1.08 (see Table 3), reflecting a weak oxidation or weak reduction environment in the Early–Middle Jurassic. In contrast, the δCe of the Daqingshan Formation ranged from 0.83 to 0.96 (see Table 3), reflecting an oxidized environment in the late Jurassic.

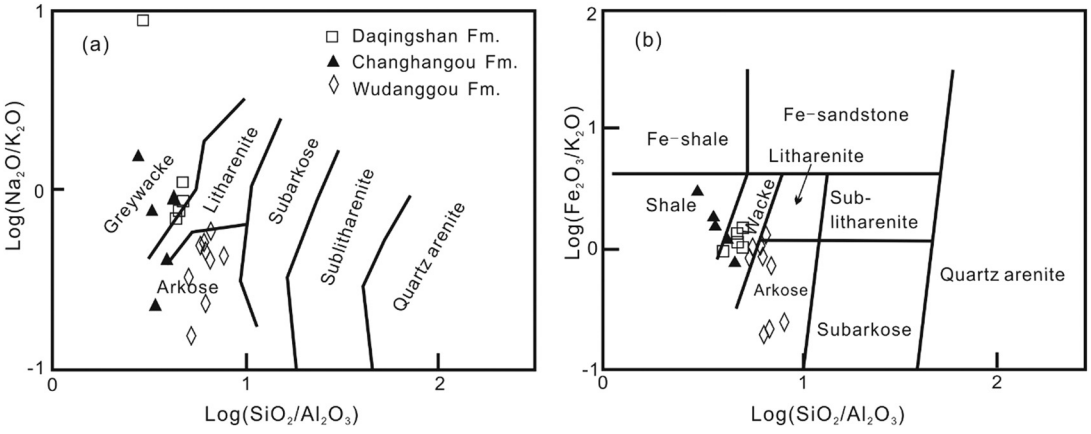

Figure 6: Chemical classification diagrams discriminating according to logarithmic ratio of SiO_2/Al_2O_3 vs Na_2O/K_2O (a: fields after ref. [55]) and Fe_2O_3/K_2O (b: fields after ref. [56]).

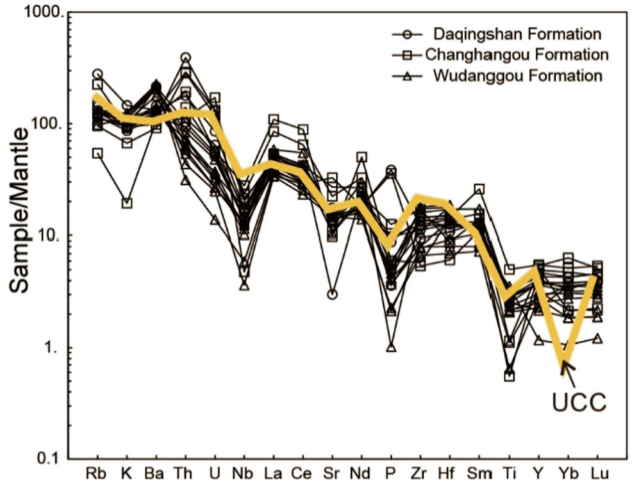

Figure 7: Primitive mantle – normalized patterns of Jurassic strata in the Daqingshan area (mantle – normalized values from ref. [60], average compositions of UCC from ref. [59]).

6 Discussion

6.1 Weathering and sediment recycling

Weathering is controlled by tectonics, climate, and terrain. Rocks during weathering causes the depletion of alkalis and alkaline earth elements [63]. Therefore, the major and trace element compositions of clastic sedimentary rocks provide constraints on physical and chemical weathering as well as sedimentary environment [58].

Feldspar minerals and alkaline silicate minerals in the rocks of the upper crust often form clay minerals such as illite and kaolinite under weathering. The unstable elemental oxides (CaO, NaO, and K_2O) are lost by weathering, whereas the content of relatively stable elemental oxides (Al_2O_3) is comparatively increased. The chemical index of alteration (CIA) [CIA = 100 × Al_2O_3/(Al_2O_3 + CaO* + Na_2O + K_2O)] reflects the quantity of weathering in the source area [64], where CaO* is the amount of CaO incorporated in the silicate mineral and was obtained herein by following MClennan's method [58]. In general, CIA values range from 60 to 77.90 (see Table 2), indicating a low-moderate degree of chemical weathering in the source area. The effect of the CIA values on potassium metasomatism during diagenesis [65] can be evaluated using an Al_2O_3–(Na_2O + CaO)–K_2O diagram [64], in which weathering trends are parallel to the Al_2O_3–(Na_2O + CaO) join, and deviations toward the K_2O apex indicate metasomatism [66]. All samples analyzed herein plot parallel to the Al_2O_3–(Na_2O + CaO) join (see Figure 9a), suggesting an intermediate degree of chemical weathering and weakly potassic metasomatism. All samples analyzed herein plot similar trends for granodiorite, adamellite, and granite, suggesting that the samples were derived from a felsic source area.

The index of compositional variability (ICV) can be used to evaluate sediment maturity [66–68]. The ICV can be calculated using the following equation: ICV = (Fe_2O_3 + K_2O + Na_2O + CaO + MgO + MnO + TiO_2)/Al_2O_3. ICV values > 1 indicate the existence of few clay minerals in the sediments and the initial deposition in the active tectonic environment. ICV values < 1 are related to alteration products such as kaolinite and illite [69,70] indicating the recycling of sediments in a passive tectonic environment or first-cycle sedimentation under high weathering. The ICV values of the Wudanggou Formation range from 0.53 to 0.90 (avg. 0.78) (see Table 2), suggesting that samples were dominated by first-cycle sedimentation in weathering. However, the ICV values of the samples from the Changhangou Formation and Daqingshan Formation range from 0.75 to 1.29 (mean = 1.04), indicating the first-cycle sediment.

U-bearing minerals are easily dissolved during weathering, whereas Th remains relatively insoluble [71,72]. The Th/U ratios in our study samples (7.03–12.24) (see Table 3) are higher than the average values for the upper crust (3.8) [1], suggesting a moderate degree of chemical weathering. Because weathering and diagenesis often lead to significant increase in Rb/Sr ratios [58], the low Rb/Sr ratios of the samples herein (mean = 0.39) suggest a low-to-moderate level of weathering history.

Hydraulic sorting can significantly influence the chemical composition of terrigenous sediments [73–76]. Similarly, SiO_2/Al_2O_3 ratios can be used to understand the textural maturity of sediments, with high values representing compositionally matured sediments [77]. The SiO_2/Al_2O_3 ratios for the Daqingshan and Changhangou Formations vary within 2.77–4.72. In contrast, for the Wudanggou Formation, the SiO_2/Al_2O_3 ratios vary within 5.11–7.75, with the higher ratios signifying the higher compositional maturity of the clastic rocks. A plot of Th/Sc against Zr/Sc can be used to distinguish the contrasting effects of source composition and sedimentary processes on the composition of clastic sedimentary rocks [58]; in such plots (see Figure 9b), all our study samples plot within the field for the upper crust. In general, the results indicate that all our samples are near-source and of low maturity.

Paleoplant fossils are direct evidence of the paleoclimate. Magpie and humid-climate plant fossils occur in the upper Wudanggou Formation, reflecting a warm and humid environment [47]. The Changhangou Formation contains

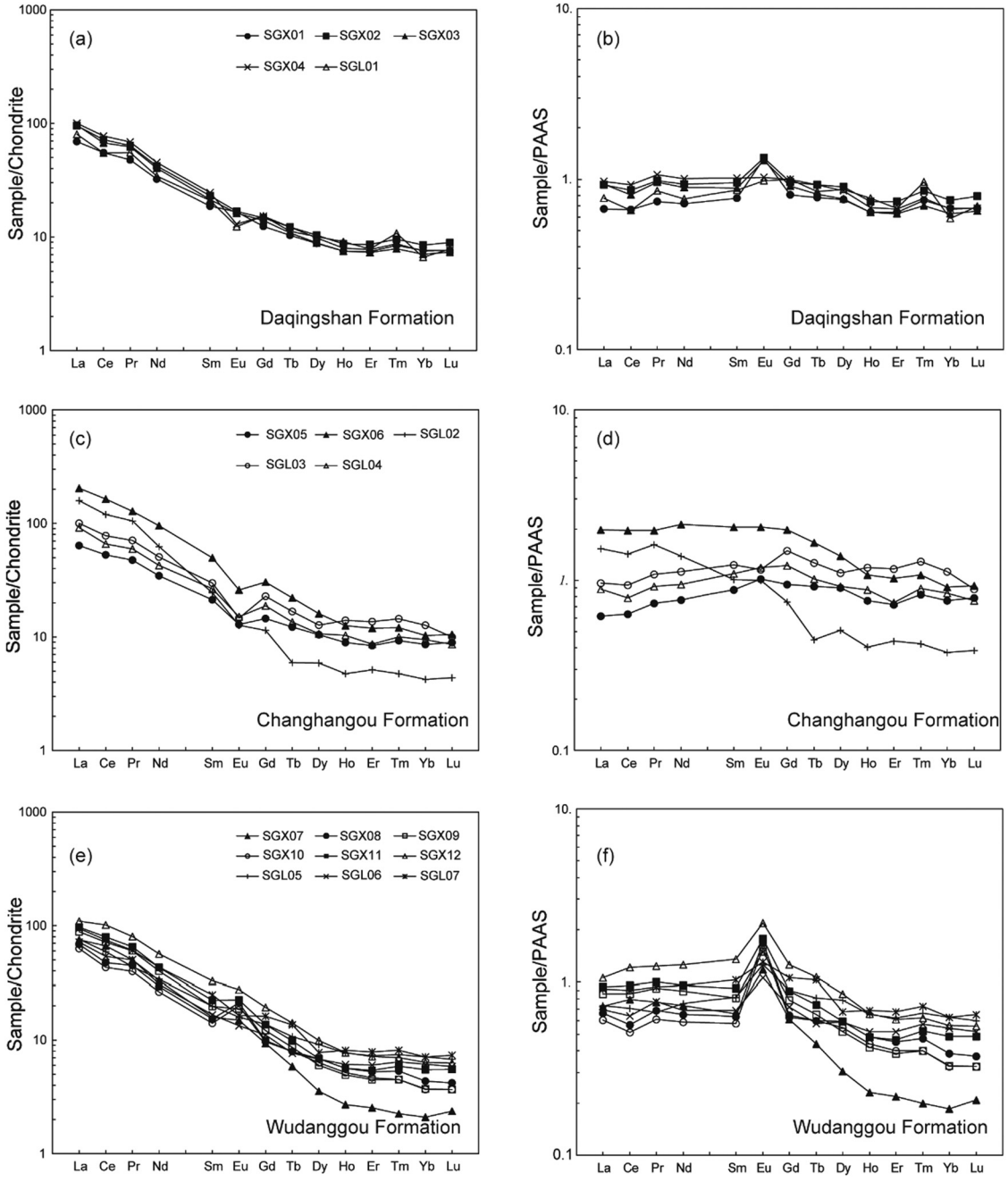

Figure 8: Chondrite and PAAS normalized REE patterns of Jurassic strata in the Daqingshan area. (a) REE normalized to chondrite for the Daqingshan Formation. (b) REE normalized to PAAS for the Daqingshan Formation. (c) REE normalized to chondrite for the Changhangou Formation. (d) REE normalized to PAAS for the Changhangou Formation. (e) REE normalized to chondrite for the Wudanggou Formation. (f) REE normalized to PAAS for the Wudanggou Formation. (chondrite-normalized values from ref. [1]; PAAS – normalized values from ref. [61]).

fossils of freshwater fish and conchostracans, also reflecting a warm and humid climate [37]. The Daqingshan Formation primarily includes purple clastic rocks that indicate an arid climate and environment. Mg/Ca ratios also can be used to indicate the paleoclimate [78]; high values represent an arid climate, and low values indicate a wet climate. The Mg/Ca ratios of our samples from the Daqingshan Formation (0.62–4.2) are greater than the average of the samples from the Wudanggou and Changhangou Formations (mean = 0.47), suggesting that the Daqingshan Formation formed in a relatively arid environment.

Table 3: Trace elements and rare earth elements concentrations in ppm on Jurassic strata in the Daqingshan area

Location	Daqingshan Formation					Changhangou Formation					Wudanggou Formation								
No	**SGX01**	**SGX02**	**SGX03**	**SGX04**	**SGL01**	**SGX05**	**SGX06**	**SGL02**	**SGL03**	**SGL04**	**SGX07**	**SGX08**	**SGX09**	**SGX10**	**SGX11**	**SGX12**	**SGL05**	**SGL06**	**SGL07**
Sr	322	291	357	63	371	691	208	470	569	228	288	318	219	307	337	283	306	289	320
V	75.8	81.0	71.6	106	95.0	57.3	125	136	105	102	44.9	29.1	53.3	22.4	71.4	84.7	65.8	77.2	46.1
Nb	10.1	11.4	9.68	12.1	15.4	3.41	19.8	16.7	12.3	14.5	12.5	4.24	8.78	2.60	8.83	9.81	9.29	8.10	7.29
Ba	1502	1006	798	927	789	737	689	888	831	637	1431	1586	1243	1446	1506	1433	937	983	891
B	18.8	23.4	11.0	143	43.2	3.90	37.2	23.9	16.7	50.8	7.42	4.22	5.77	7.24	8.51	8.70	5.62	6.93	4.15
Th	8.74	9.49	7.95	15.1	33.3	9.46	11.9	24.7	16.4	24.1	6.25	2.66	4.56	3.69	5.42	7.14	4.93	5.17	6.09
U	1.13	1.35	1.07	1.79	2.72	3.60	1.19	2.79	1.17	2.46	0.75	0.29	0.56	0.52	0.66	1.00	0.56	0.78	0.69
Rb	90.9	98.7	71.7	177	74.5	34.4	143	80.3	76.5	60.5	77.4	78.7	68.7	79.5	83.9	78.3	80.6	78.7	62.0
Sc	10.8	13.2	9.70	13.5	12.9	13.3	13.7	18.8	17.4	15.8	9.75	5.84	8.93	5.53	13.4	11.5	6.36	8.90	7.22
Hf	4.26	3.88	4.68	3.32	3.86	1.89	4.43	3.59	4.29	2.68	5.75	2.49	5.49	2.17	4.57	5.28	2.86	5.62	4.13
Ta	0.44	0.54	0.39	0.56	0.48	0.48	0.93	0.58	0.83	0.68	0.48	0.24	0.31	0.10	0.28	0.35	0.32	0.25	0.29
Co	15.7	17.4	13.6	8.77	12.6	6.90	20.7	24.4	25.3	24.3	4.45	10.2	8.54	5.75	7.68	12.1	7.26	7.33	5.91
Cr	50.0	54.7	46.0	97.0	67.9	20.8	128	93.3	109	65.9	52.1	22.3	54.1	20.9	53.1	51.9	42.9	34.7	46.1
Ni	29.3	35.2	24.9	32.4	26.9	16.9	51.5	45.5	40.6	36.5	7.06	17.6	15.8	13.0	20.3	27.4	13.5	12.8	10.7
Zr	139	124	159	105	136	60.6	148	160	65.3	191	200	89.0	192	75.2	162	178	87.2	119	90.2
Y	17.2	19.8	17.2	17.6	18.6	21.4	25.2	23.6	24.8	22.6	5.32	14.5	9.81	12.6	11.4	16.6	12.6	13.8	10.4
La	25.4	35.1	35.5	36.8	29.4	23.4	74.9	58.3	36.7	33.7	27.6	25.1	32.5	23.1	35.6	40.2	27.9	26.4	34.7
Ce	52.9	68.9	64.5	74.0	52.6	50.6	157	114	74.7	63.0	63.5	45.3	68.4	41.2	76.1	97.0	56.6	51.3	71.6
Pr	6.54	8.74	8.52	9.41	7.58	6.50	17.5	14.4	9.69	8.17	6.85	6.13	8.23	5.44	8.92	11.0	5.98	6.90	8.32
Nd	23.0	30.0	28.7	32.2	24.5	24.6	67.9	44.4	36.0	30.4	23.5	20.9	28.4	18.8	30.5	40.2	24.1	21.9	30.7
Sm	4.32	5.33	4.94	5.69	4.84	4.91	11.5	5.66	6.89	6.15	3.67	3.55	4.56	3.25	5.16	7.58	4.58	3.86	5.76
Eu	1.45	1.46	1.41	1.13	1.08	1.12	2.26	1.10	1.28	1.31	1.30	1.85	1.64	1.73	1.96	2.41	1.39	1.17	1.43
Gd	3.79	4.51	4.28	4.67	4.69	4.45	9.31	3.49	6.99	5.75	2.86	3.03	3.71	2.96	4.19	5.92	4.20	3.39	4.96
Tb	0.60	0.71	0.63	0.71	0.65	0.71	1.28	0.34	0.97	0.79	0.34	0.46	0.50	0.46	0.57	0.82	0.62	0.44	0.79
Dy	3.35	3.95	3.38	3.74	3.84	3.99	6.11	2.24	4.84	4.06	1.35	2.61	2.29	2.41	2.62	3.77	3.48	2.59	2.96
Ho	0.64	0.74	0.64	0.68	0.77	0.76	1.07	0.40	1.19	0.88	0.23	0.48	0.42	0.44	0.48	0.66	0.65	0.52	0.69
Er	1.85	2.14	1.82	1.93	1.95	2.09	2.97	1.28	3.39	2.15	0.63	1.31	1.12	1.16	1.35	1.78	1.81	1.50	1.96
Tm	0.30	0.34	0.28	0.31	0.38	0.33	0.43	0.17	0.52	0.36	0.08	0.19	0.16	0.16	0.21	0.25	0.26	0.23	0.29
Yb	1.89	2.11	1.75	1.87	1.65	2.13	2.55	1.05	3.15	2.35	0.52	1.08	0.92	0.91	1.36	1.58	1.77	1.52	1.76
Lu	0.29	0.34	0.28	0.29	0.30	0.34	0.40	0.17	0.38	0.33	0.09	0.16	0.14	0.14	0.21	0.24	0.26	0.22	0.28
δEu	1.10	0.91	0.94	0.67	0.69	0.73	0.67	0.76	0.56	0.67	1.23	1.72	1.22	1.70	1.29	1.10	0.97	0.99	0.82
δCe	0.96	0.92	0.87	0.93	0.83	0.96	1.02	0.92	0.93	0.89	1.08	0.86	0.98	0.86	1.00	1.08	1.03	0.89	0.99
ΣREE	126	164	157	173	134	126	355	247	187	159	133	112	153	102	169	213	134	122	166
LREE/HREE	8.94	10.1	11.0	11.2	8.43	7.51	13.7	26.0	7.71	8.56	20.7	11.0	15.5	10.8	14.4	13.2	9.23	10.7	11.1
$(La/Yb)_n$	9.08	11.2	13.7	13.3	12.1	7.42	19.8	19.8	7.89	9.69	35.9	15.7	23.9	17.2	17.7	17.2	10.7	11.7	13.3

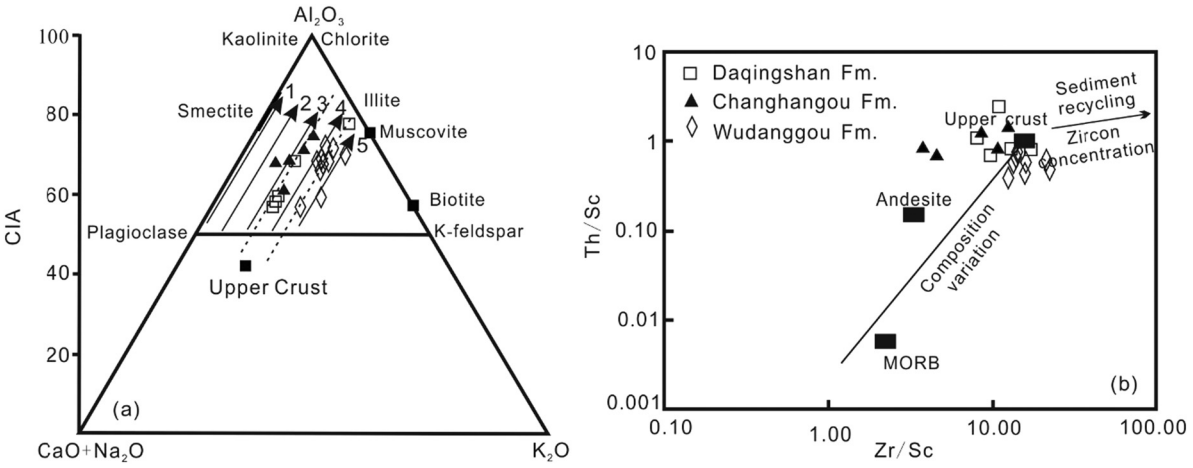

Figure 9: (a) A–CN–K ternary diagram of molecular proportions of Al_2O_3–(CaO + Na_2O)–K_2O for Jurassic sedimentary rock (fields after ref. [64]). Also plotted is the average continental crust [1]. Arrows 1–5 represent the weathering trends of gabbro, tonalite, granodiorite, adamellite and granite, respectively [64]. (b) Th/Sc vs Zr/Sc bivariate plot of Jurassic sedimentary rock (fields after ref. [58]).

6.2 Source area

6.2.1 Clastic composition of gravels

The composition of clastic rocks reflects the tectonic setting of a source area and sedimentary basin. The content of gravel with different components, sizes, and tendencies can be used to distinguish the lithology of the source, transportation distance, and paleocurrent.

The grain size of detrital materials on the Baicaigou section in the northern margin of the basin generally exhibited a decreasing trend from boulder conglomerate (North) to shale (South) (see Figure 3). The dip in imbricated gravel from the Daqingshan Formation on the north of the basin shows a dominant paleocurrent direction toward the south [79]. The dip in imbricated gravel and cross-stratification from the Baicaigou section shows a dominant paleocurrent direction toward the southwest [31]. The dip of cross-stratification from the Haimaban section and Yankeleng outcrop belt in the south of the basin show a dominant paleocurrent direction toward the northeast and northwest, respectively [31]. The results suggest sediment source from the northern and southern margins of the basin.

Gravel selected from the Jurassic strata was used for statistical analyses (see Figure 3). The bottom gravel of the Wudanggou Formation mainly contained gneiss together with a small amount of pegmatite, granite, and diabase. The conglomerate composition of the Changhangou Formation is complex, in which gneiss is the most abundant, followed by marble, few silicalites, and quartzite. The gravel composition of the Daqingshan Formation is mostly gneiss, followed by quartzite and silicalite. Thus, it can be inferred that the Archaean gneiss around the basin is one of the main provenance areas.

6.3 Geochemical

Most femic elements such as Fe, Ti, Mg, Sc, Co, Cr, Ni, and V in addition to small ionic elements such as Na, Ca, and Sr are enriched in basic rocks and their weathered products, whereas elements such as K, Rb, Pb, and REEs as well as high valence ions such as Th, U, Zr, and Nb are more enriched in felsic rocks and their weathered products [58]. The La/Sc, Th/Sc, La/Co, Th/Co, and Th/Cr ratios are particularly sensitive to the average source composition [1]. Some significant differences in elemental ratio populations from different areas exist, suggesting some local control of source rocks on sediment composition. The variable ratio suggests mainly the sediments of Jurassic sandstones originated from felsic sources (see Table 4).

Ni (ppm) vs TiO_2 (wt%) indicates that the analyzed samples plot predominantly to the field of felsic area rather than those of mafic igneous or sedimentary origin (see Figure 10a) [80]. On the plot of La/Sc vs Co/Th (see Figure 10b), the Co/Th ratios of all studied samples are nearly 1.27 and close to those of felsic volcanic rocks [1]. Floyd and Leveridge established a discrimination diagram using La/Th vs Hf (see Figure 10c) to determine different arc components and sources [81]. Uniform low La/Th ratios and Hf contents of samples from the Changhangou and Daqingshan Formations suggest derivation,

Table 4: Range of elemental ratios of samples compared with ratios in similar fractions derived from felsic and mafic rocks and UCC [1]

	Daqingshan Fm.	Changhangou Fm.	Wudanggou Fm.	Sediments from felsic source	Sediments from mafic source	Upper continent crust
La/Sc	2.29–3.66	1.76–5.47	2.66–4.81	2.50–16.3	0.43–0.86	2.21
Th/Sc	0.72–2.59	0.71–1.53	0.40–0.84	0.84–20.5	0.05–0.22	0.79
La/Co	1.62–4.20	1.35–3.62	2.46–6.20	1.80–13.8	0.14–0.38	1.76
Th/Co	0.55–2.65	0.65–1.37	0.26–1.40	0.67–19.4	0.04–1.40	0.63
Th/Cr	0.16–0.49	0.09–0.45	0.08–0.18	0.067–4.0	0.002–0.045	0.13

predominantly from a felsic arc source, whereas the samples from the Wudanggou Formation were controlled by a mixed felsic and mafic source.

REEs exhibit similar chemical properties, mainly controlled by the rock components in the source area and are weakly affected by weathering, diagenesis, and alteration; in addition, they can reflect the REE characteristics of the source rocks [1,64]. The relationship between the La/Yb ratio and ∑REE content can reflect the genetic characteristics of rock types [58]. The La/Yb–∑REE diagram (see Figure 10d) shows that most samples plot to the sedimentary rock area and sedimentary rock–granite overlap area in addition to few plots in the granite area, indicating that the basin source mainly originates from the upper crust felsic source area.

6.4 Tectonic setting

The geochemical characteristics of sediments are closely related to their provenance and tectonic setting. The geochemical composition of the sedimentary rocks is formed under different tectonic settings. Although some established discrimination diagrams are not really significant

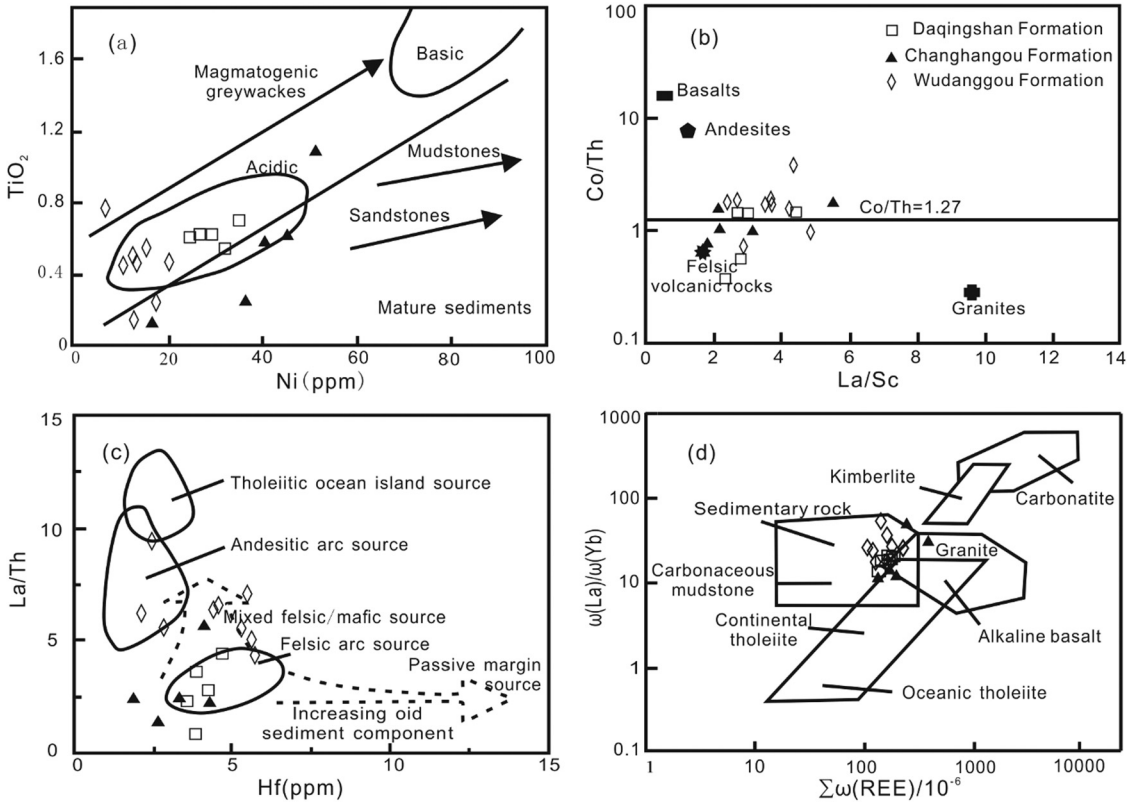

Figure 10: Source rock discrimination diagrams with trace elements for Jurassic strata in the Daqingshan area. (a) TiO_2 vs Ni diagram (fields after ref. [82]); (b) Co/Th vs La/Sc diagram (fields after ref. [83]); (c) La/Th vs Hf diagram (fields after ref. [81]); (d) La/Yb vs ∑REE diagram (fields after ref. [81]). Average compositions of volcanic rocks in plot (b) from ref. [84]).

for specific local plate tectonic settings [85], the geochemical compositions of sediments have been widely used to infer the plate tectonic setting of ancient sedimentary basins [1,56,86,87].

Comparison between the distribution curve of chondrite normalized to the REE average value and four typical tectonic backgrounds [88] shows that the source area exhibited similar continental island arc and/or active continental margin tectonic setting (see Figure 11a).

Bhatia developed useful and effective discriminant functions to infer tectonic settings [88]. All samples from the Wudangghou Formation plot in the active continental margin, whereas the samples from the Changhangou and Daqingshan Formations mainly plot in the continental island arc and active continental margin (see Figure 11b). Roser and Korsem used the K_2O/Na_2O vs SiO_2 to resolve the tectonic setting of clastic sedimentary rocks [85]. SiO_2 and K_2O/Na_2O increase from the volcanic arc to the active continental margin to the passive margin situation. All samples from the Wudangghou Formation fall into the passive continental margin field, whereas the samples from the Changhangou and Daqingshan Formations mainly fall into the passive and active continental margin (see Figure 11c). On a plot of K_2O/Na_2O vs SiO_2/Al_2O_3 (see Figure 11d), samples from the Wudangghou Formation fall into the field of a passive continental margin, in contrast, the samples from the Changhangou and Daqingshan Formations mainly fall into the passive and active continental margins.

Some trace elements in sediments are inactive and exhibit slight changes during the deposition process. The source rock and weathering conditions are the main factors controlling the trace elements in the sediments. Some of these elements can reflect the tectonic setting of the sedimentary basin [2]. La, Th, Zr, Nb, Y, Sc, Co, and Ti are highly effective for distinguishing different

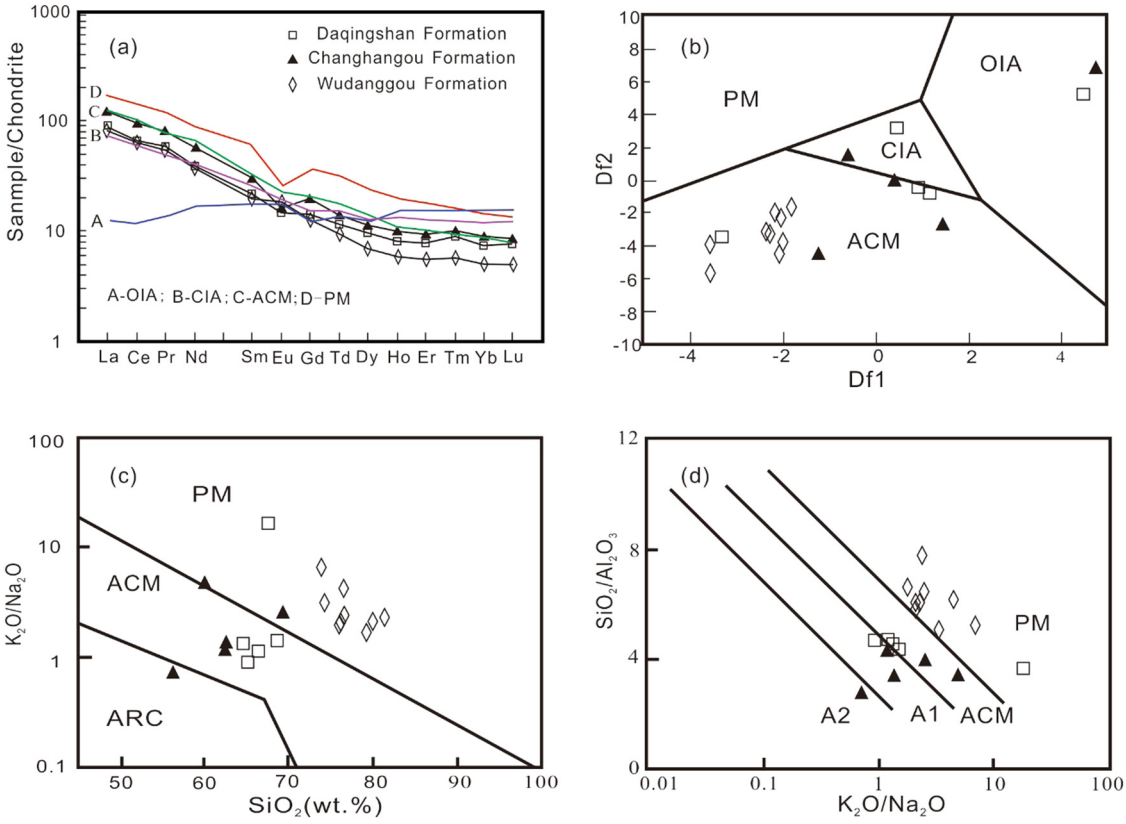

Figure 11: (a) Comparison diagram of chondrite-normalized REE patterns of Jurassic strata in the Daqingshan area and various tectonic setting (fields after ref. [89]); (b) discriminant function diagram (fields after ref. [89]); (c) K_2O/Na_2O vs SiO_2 diagram (fields after ref. [85]); (d) SiO_2/Al_2O_3 vs K_2O/Na_2O diagram (fields after ref. [90]). ACM = active continental margin; PM = passive continental margin; CIA = continental island arc; OIA = oceanic island arc; A1 = evolved arc setting, with supply of felsic–plutonic detritus; A2 = arc setting, with supply of basaltic and andesitic detritus discriminant functions are: $Df1 = -0.0447 \times SiO_2 - 0.972 \times TiO_2 + 0.008 \times Al_2O_3 + 0.267 \times Fe_2O_3 + 0.208 \times FeO - 3.082 \times MnO + 0.14 \times MgO + 0.195 \times CaO + 0.719 \times Na_2O - 0.032 \times K_2O + 7.510 \times P_2O_5 + 0.303$; $Df2 = -0.421 \times SiO_2 + 1.988 \times TiO_2 - 0.526 \times Al_2O_3 - 0.551 \times Fe_2O_3 - 1.61 \times FeO + 2.72 \times MnO + 0.881 \times MgO - 0.90 \times CaO - 0.177 \times Na_2O - 1.84 \times K_2O + 7.244 \times P_2O_5 + 43.57$.

tectonic settings [57]. Co, Sc, and Zr exhibit good stability. Sc and Co are compatible elements, demonstrating a good correlation, representing the immature tectonic background. The large ion lithophile element Th represents the immature tectonic background, and Zr indicates sedimentation degree [57]. Th–Sc–Zr/10, Th–Co–Zr/10, and La–Th–Sc discriminant diagrams show that most of the samples plot to the continental island arc field, few plot to the active continent margin, and some samples plot to the blank area around the continental island arc and active continent margin [50]. In general, source regions mainly exhibit continental island arc and/or active continental margins (see Figure 12). Tectonic setting discriminant diagrams based on the major element are different from those of the trace elements and REEs. K_2O and Na_2O are easily lost during weathering, whereas REEs and Th, Co, and Zr are relatively stable. Comprehensive analysis suggests that the source rock is mainly from active continental margins and continental island arc. This further suggests that the samples were derived from complex source regions.

The northern margin of the NCC has experienced a history of continental margin evolution on the south side of the Ancient Asian Ocean from Neoarchean to Late Paleozoic [51,91,92]. U–Pb dating of zircons revealed multiple magmatic age peaks at ca. 2,450–2,500, 2,100–2,300, 1,930–1,970, and 1,850 Ma, and metamorphic ages at ca. 1,900 Ma, indicating multiple magmatic and metamorphic events in the Daqingshan–Wulashan area [27,93]. The Khondalite belt underwent long-term arc – continent accretion along the southern margin of the Yinshan Block during the late Neoarchean–Paleoproterozoic, and terminal continent – continent collision of the Yinshan and Ordos Blocks at ca. 1.90–1.95 Ga [20,25–27,94,95]. Therefore, we infer that the Archean–Proterozoic basement provided continental island arc material for the basin. The Early Paleozoic Bainaimiao arc belt was built on a

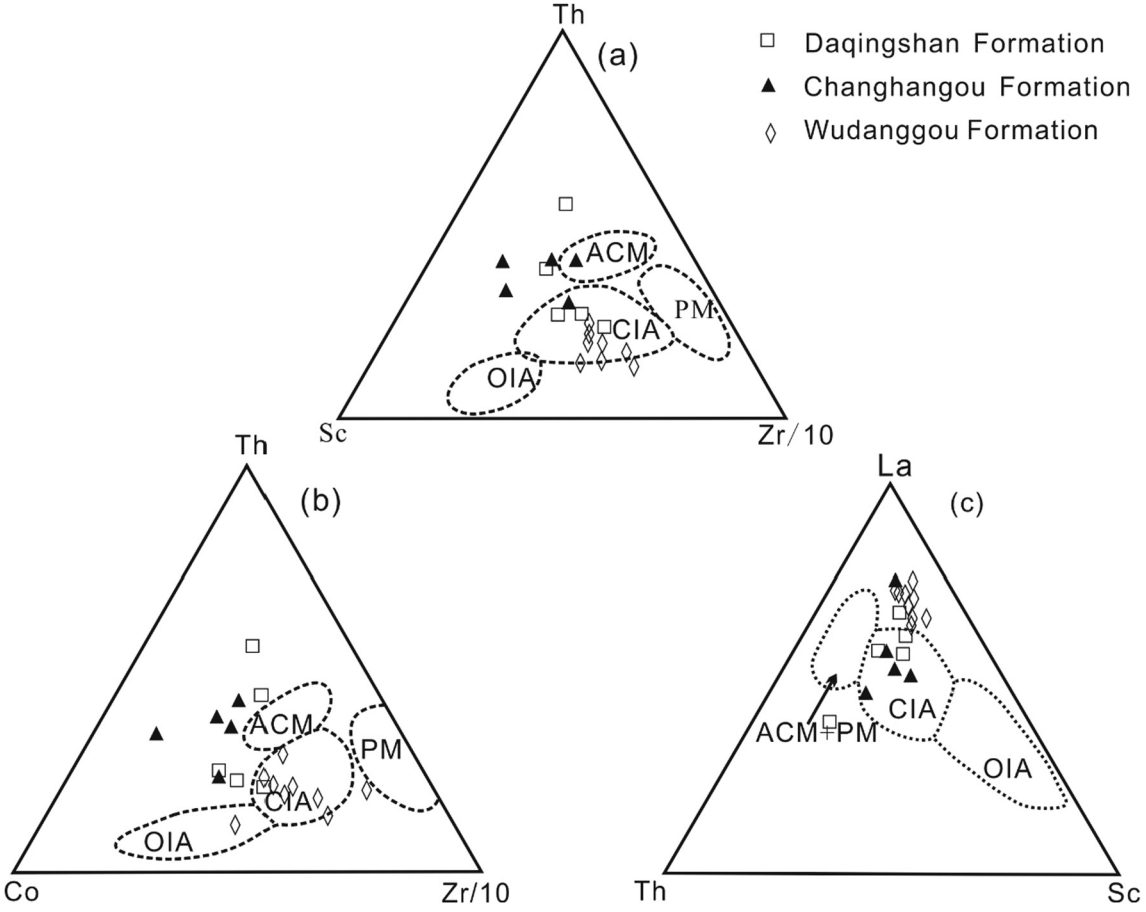

Figure 12: Tectonic setting discrimination diagrams with trace elements for the Jurassic strata in the Daqingshan area (fields after ref. [57]). (a) Th–Sc–Zr/10 plots; (b) Th–Co–Zr/10 plots; (c) La–Th–Zr/10 plots. OIA = oceanic island arc; CIA = continental island arc; ACM = active continental margin; PM = passive margin.

Precambrian microcontinent that has a tectonic affinity to the Tarim or Yangtze Cratons and was accreted to the northern NCC during the Late Silurian–Early Devonian by arc–continent collision [96]. The northern margin of the NCC has changed from passive to active continental margin. Additionally, massive I-type intrusion and volcanism during Carboniferous–Permian time indicates that the northern margin of the NCC is an Andean-type active continental margin and the locus of southward subduction of the Paleo-Asian oceanic plate beneath the northern NCC [97,98]. We infer that Carboniferous–Permian volcanic rocks have provided material for the basin's active continental margins.

7 Conclusion

The following are the conclusions drawn from the field interaction, petrography, and geochemistry studies of the samples:

The average modal composition classifies the samples as wacke or arkose and is also supported by geochemical studies. The Jurassic strata generally exhibit a low-to-medium degree of weathering, with near source and low maturity. The Wudanggou and Changhangou Formations areas exhibit a warm and humid environment, whereas the Daqingshan Formation showed an acidic environment. The chondrite-normalized pattern of the samples shows high LREE content. Samples from the Wudanggou Formation show pronounced positive Eu anomalies, and samples from the Changhangou and Daqingshan Formations exhibit pronounced negative Eu anomalies.

Petrographic and geochemical data obtained from the studied samples indicate that felsic volcanic rocks and the Precambrian basement were the most important source rock for all samples; however, few mafic materials may have been contributed to the Wudanggou Formation. The geochemical information interpretation on various diagrams reveals the source material to be from the active continent margin and continental island arc settings. The Archean–Proterozoic basement provides material for the basin as continental island arc, and Carboniferou–Permian volcanic rocks provide material for the basin as active continental margins.

The Changhangou Formation unconformably overlies the Wudanggou Formation and with different petrological and geochemical, source areas, and tectonic settings. This shows that the Yanshanian movement influenced the formation of the Changhangou formation and the initiation of the Yanshanian movement should be earlier than 163.7 ± 1.0 Ma, rather than the end of the Middle Jurassic.

Author contributions: Conceptualization, Zhang, MJ, Yu, YQ; Methodology, Zhang, MJ, and Cai, K and Shi, MY; Visualization, Zhang, MJ, Yu, YQ; Writing-original draft preparation, Zhang, MJ; Writing-review and editing, Choi, JY, Cai, K; All authors have read and agreed to the published version of the manuscript. This work represents part of Zhang, MJ.'s Doctorate Research performed at the Kunshan National University.

Acknowledgments: We sincerely appreciate the editors and reviewers for constructive comments. We also thank Dr. Chio Taejin who critically read the early draft and helped with geochemical analyzes. This study was financially supported by the Geological Investigation Project of Inner Mongolia (NMKD2013-24) and the PM60040 Research grant from the Korea Institute of Ocean Science and Technology (KIOST).

References

[1] Taylor SR, McLennan SM. The continental crust: Its composition and evolution. An Examination of the Geochemical Record Preserved in Sedimentary Rocks. Oxford: Oxford University, Blackwell Scientific Pub; 1985. p. 312.
[2] McLennan SM, Taylor SR. Sedimentary rocks and crustal evolution: tectonic setting and secular trends. J Geol. 1991;99(1):1–21.
[3] Critelli S, Arribas J, Le Pera E, Tortosa A, Marsaglia KM, Latter KK. The recycled orogenic sand provenance from an uplifted thrust-belt, Betic Cordillera, southern Spain. J Sediment Res. 2003;73(1):72–81.
[4] Critelli S. Provenance of Mesozoic to Cenozoic Circum-Mediterranean sandstones in relation to tectonic setting. Earth-Science Rev. 2018;85:624–48.
[5] Davis GA, Wang C, Zheng YD, Zhang JJ, Zhang CH, Gehrels GE. The enigmatic Yinshan fold-and-thrust belt of Northern China: New views on its intraplate contractional styles. Geology. 1998;26(1):43.
[6] Davis GA, Darby BJ, Zheng YD, Spell TL. Geometric and temporal evolution of an extensional detachment fault, hohhot metamorphic core complex, Inner Mongolia, China. Geology. 2002;30(11):1003–6.
[7] Chen ZY, Wen CS, Zhang WJ. Nappe structure in Mount Seerteng. Inn Mong Earth Sci. 2000;25:237–41 (in Chinese with English abstract).
[8] Liu ZH, Xu ZY, Yang ZS. On Dagingshang thrust – nappe in Inner Mongolia. Regional Geology China. 1999;18(4):366–72 (in Chinese with English abstract).
[9] Liu ZH, Xu ZY, Yang ZS. Daqingshan thrust system signification and its geological characteristics. World Geology. 2001;3:224–30 (in Chinese with English abstract).

[10] Xu ZY, Liu ZH, Yang ZS, Wu XW, Chen XF. Structure of metamorphic strata of the khondalite series in the Daqingshan-Wulashan area, central Inner Mongolia, China, and their geodynamic implications. Geol Bull China. 2007;26(5):526–36 (in Chinese with English abstract).
[11] Cai J, Liu PH, Liu FL, Liu JH, Wang FL, Shi JR. Genetic mineralogy and metamorphic evolution of Al-rich gneisses in the Shiguai area, Daqingshan-Wulashan metamorphic complex belt. Acta Petrologica Sin. 2013;29(2):437–61 (in Chinese with English abstract).
[12] Song HF, Xu ZY, Liu ZH. Geochemical characteristics and origin of garnet migmatitic granites in Daqingshan area. Inn Mong Acta Petrologica Et Mineralogica. 2005;24(5):489–95 (in Chinese with English abstract).
[13] Xu ZY, Liu ZH, Hu FX, Yang ZS. Geochemical characteristics of the calc-silicate rocks in khondalite series in Daqingshan area. Inn Mong J Jilin Univ (Earth Sci Ed). 2005;35(6):681–9 (in Chinese with English abstract).
[14] Zhong CT, Deng JF, Wu YP, Mao DB, Xi Z, Cheng B. Geochemical characteristics and tectonic significations of Paleoproterozoic strongly peraluminous granitoids in the central segment of the northern margin of the North China Craton. Geol Bull China. 2006;25(3):389–97 (in Chinese with English abstract).
[15] Tao JX. Characteristics of Neoarchean metamorphic intrusives and the relationship with the mineralization of gold in Guyang region, Inner Mongolia. Geological Survey. Research. 2003;26(1):21–6 (in Chinese with English abstract).
[16] Jian P, Zhang QC, Liu DY, Jin WJ, Jia XQ, Qian Q. SHRIMP dating and geological significance of Late Achaean high-Mg diorite (sanukite) and hornblende-granite at Guyang of Inner Mongolia. Acta Petrologica Sin. 2005;21(1):151–7 (in Chinese with English abstract).
[17] Wu CH, Sun M, Li HM, Zhao GC, Xia XP. LA-ICP-MS U-Pb zircon ages of the khondalites from the Wulashan and Jining high-grade terrain in northern margin of the North China Craton: Constraints on sedimentary age of the khondalite. Acta Petrologica Sin. 2006;22(11):2639–54 (in Chinese with English abstract).
[18] Xia XP, Sun M, Zhao GC, Wu FY, Xu P, Zhang JH, et al. U–Pb and Hf isotopic study of detrital zircons from the Wulashan khondalites: constraints on the evolution of the Ordos Terrane, Western Block of the North China Craton. Earth Planet Sci Lett. 2006;241(3–4):581–93.
[19] Ma MZ, Wan YS, Santosh M, Xu ZY, Xie HQ, et al. Decoding multiple tectonothermal events in zircons from single rock samples: SHRIMP zircon U-Pb data from the late Neoarchean rocks of Daqingshan, North China Craton. Gondwana Res. 2012;22(3–4):810–27.
[20] Dong CY, Wan YS, Wilde SA, Xu ZY, Ma MZ, Xie HQ, et al. Earliest Paleoproterozoic supracrustal rocks in the North China Craton recognized from the Daqingshan area of the Khondalite belt: Constraints on craton evolution. Gondwana Res. 2014;25(4):1535–53.
[21] Dong CY, Wan YS, Long T, Zhang YH, Liu JH, Ma MZ, et al. Oxygen isotopic compositions of zircons from Paleoproterozoic metasedimentary rocks in the Daqingshan-Jining area, North China Craton: In situ SHRIMP analysis. Acta Petrologica Sin. 2016;32:659–81 (in Chinese with English abstract).
[22] Hu B, Zhai MG, Peng P, Liu F, Diwu CR, Wang HZ, et al. Late Paleoproterozoic to Neoproterozoic geological events of the North China Craton: Evidences from LA-ICP-MS U-Pb geochronology of detrital zircons from the Cambrian and Jurassic sedimentary rocks in Western Hills of Beijing. Acta Petrologica Sin. 2013;29(7):2508–36 (in Chinese with English abstract).
[23] Wan YS, Xu ZY, Dong CY, Nutman A, Ma MZ, Xie HQ, et al. Episodic Paleoproterozoic (2.45, 1.95 and 1.85 Ga) mafic magmatism and associated high temperature metamorphism in the Daqingshan area, North China Craton: SHRIMP zircon U–Pb dating and whole-rock geochemistry. Precambrian Res. 2013;224:71–93.
[24] Liu JH, Liu FL, Ding ZJ, Chen JQ, Liu PH, Shi JR, et al. Zircon U-Pb chronology, geochemistry and their petrogenesis of Early Paleoproterozoic granitoid gneisses in Ulashan area, North China Craton. Acta Petrologica Sin. 2013;29(2):485–500 (in Chinese with English abstract).
[25] Liu JH, Liu FL, Ding ZJ, Chen JQ, Liu PH, Cheng JQ, et al. Late Neoarchean–Paleoproterozoic arc-continent accretion along the Khondalite Belt, Western Block, North China Craton: Insights from granitoid rocks of the Daqingshan–Wulashan area. Precambrian Res. 2017;303:494–519.
[26] Liu PH, Liu FL, Cai J, Liu JH, Shi JR, Wang F. Geochronological and geochemical study of the Lijiazi mafic granulites from the Daqingshan-Wulashan metamorphic complex, the central Khondalite Belt in the North China Craton. Acta Petrologica Sin. 2013;29(2):922–42.
[27] Liu PH, Liu FL, Liu CH, Liu JH, Wang F, Xiao LL, et al. Multiple mafic magmatic and high-grade metamorphic events revealed by zircons from meta-mafic rocks in the Daqingshan–Wulashan Complex of the Khondalite Belt, North China Craton. Precambrian Res. 2014;246:334–57.
[28] Liu PH, Liu FL, Cai J, Yang H, Wang F, Liu CH, et al. Metamorphic P-T conditions and timing of the Wuchuan garnet mafic granulite from the Yinshan Block, North China Craton: Insight from phase equilibria and zircon U-Pb dating. Acta Petrologica Sin. 2016;32(7):1949–79 (in Chinese with English abstract).
[29] Cai J, Liu FL, Liu PH, Wang F, Shi JR. Geochronology of the Paleoproterozoic khondalite rocks from the Wulashan-Daqingshan area, the Khondalite Belt. Acta Petrologica Sin. 2015;31(10):3081–106 (in Chinese with English abstract).
[30] Chen PJ, Dai CC, Huang C, Huang XL. Geochemical characteristics and zircon U-Pb age of the Paleoproterozic S-type granite in Wulashan region and its geological significance. Geol China. 2017;44(5):959–73 (in Chinese with English abstract).
[31] Ritts D, Darby BJ, Cope T. Early Jurassic extensional basin formation in the Daqing shan segment of Yinshan belt, Northern North China Block, Inner Mongolia. Tectonophysics. 2001;339:239–58.
[32] Liu ZH, Xu ZY. Indosinian Tectonic Movement in the Daqingshan Region in Inner Mongolia. Geol Rev. 2003;49(5):457–63 (in Chinese with English abstract).
[33] Peng XD, Xu ZY, Liu ZH. The Formation, Movement and Evolution Pattern of Jurassic Terrestrial Deposit Basin in Daqingshan Region. Word Geol. 2001;4(2):105–10.
[34] Xu XJ, Zhao YJ. Discussion on the Formation and Origin of the Shiguai Mesozoic Rift Basin in Inner Mongolia. J Jiling Univ (Earth ence Ed). 2005;1:33–8 (in Chinese with English abstract).

[35] Zhao Y, Zhang SH, Xu G, Yang ZY, Hu JM. The Jurassic major tectonic events of the yanshan intraplate deformation belt. Regional Geol China. 2004;23(9–10):854–63.
[36] Zhao Y, Zhai MG, Chen H, Zhang SH. Paleozoic-early Jurassic tectonic evolution of North China Craton and its adjacent orogenic belts. Geol China. 2017;44(1):44–60 (in Chinese with English abstract).
[37] Wang Y, Dong S, Shi W, Chen X, Jia L. The Jurassic structural evolution of the western Daqingshan area, Eastern Yinshan belt, North China. Int Geol Rev. 2017;59(15):1–23.
[38] Zhang JJ, Qi GW, Guo L, Liu J. 40Ar–39Ar dating of the mesozoic thrusting in Daqingshan thrust-nappe system, Inner Mongolia, China. Acta Petrologica Sin. 2009;25(3):609–20 (in Chinese with English abstract).
[39] Zhao GC, Sun M, Wilde SA, Li SZ. Late Archean to Paleoproterozoic evolution of the North China Craton: Key issues revisited. Precambrian Res. 2005;136(2):177–202.
[40] Du JM, Zhang QL, Xu SY, Du SX. Characters of later Jurassic Yinshan intraplate orogeny belt-evidence from Daqing Shan. Inn Mong Acta Geologica Sin. 2009;83(7):910–922 (in Chinese with English abstract).
[41] Darby BJ, Davis GA, Zheng YD. Structural evolution of the southwestern Daqing Shan, Yinshan Belt, Inner Mongolia. China, Geol Soc Am Mem. 2001;194:199–214.
[42] Zhang SH, Zhao Y, Ye H, Hou KJ, Li CF. Early Mesozoic alkaline complexes in the northern North China craton: Implications for cratonic lithospheric destruction. Lithos. 2012;155:1–18.
[43] Liu SF, Su S, Zhang GW. Early Mesozoic basin development in North China: Indications of cratonic deformation. J Asian Earth Sci. 2013;62:221–36.
[44] Li ZH, Dong SW, Qu HJ. Timing of the initiation of the Jurassic Yanshan movement on the North China craton: Evidence from sedimentary cycles, heavy minerals, geochemistry, and zircon U–Pb geochronology. Int Geol Rev. 2013;56:288–312.
[45] Meng QR, Wei HH, Wu GL, Duan L. Early Mesozoic tectonic settings of the northern North China craton. Tectonophysics. 2014;611:155–66.
[46] Liu J, Zhao Y, Liu XM, Wang Y, Liu XW. Rapid exhumation of basement rocks along the northern margin of the North China craton in the Early Jurassic: Evidence from the Xiabancheng Basin, Yanshan Tectonic Belt. Basin Res. 2012;24: 544–58.
[47] Li ZH, Feng SB, Yuan XQ, Qu HJ. Chronology and its significance of the Lower Jurassic tuff in Ordos Bain and its periphery. Oil Gas Geology. 2014;35:729–41 (In Chinese with English abstract).
[48] Ge YH, Sun CL, Wang YF. The flora from Zhaogou Formation in Shiguai basin, Inner Mongolia and the geological age. Global Geology. 2010;29:175–82 (In Chinese with English abstract).
[49] Zhang H, Yuan HL, Hu ZC, Liu XM, Diwu CR. U-Pb zircon dating of the Mesozoic volcanic strata in Luanping of North Hebei and its significance. Earth Sci. 2005;6:707–20 (in Chinese with English abstract).
[50] Shao JA, Meng QR, Wei HQ, Zhang LQ, Wang PY. Nature and tectonic environment of late Jurassic volcanic-sedimentary basins in northwestern hebei province. Regional Geol China. 2003;22(10):751–61 (in Chinese with English abstract).
[51] Xu H, Liu YQ, Kuang HW, Liu YX, Peng N, Dong C, et al. Sedimentay provenance and basin evolution of Daqingshan Formation. Houcheng Formation Tuchengzi Formation Yinshan-Yanshan area Geol Bull China. 2013;32(2):502–24 (in Chinese with English abstract).
[52] Ingersoll RV, Bullard TF, Ford RL, Grimm JP, Pickle JD, Sares SW. The effect of grain size on detrital modes; a test of the Gazzi-Dickinson pointcounting method. Sediment Res. 1984;54(1):103–16.
[53] Folk RL, Andews PB, Lewis DW. Detrital sedimentary rock classificationand nomenclature for use in New Zealand. New Zealand J Geol Geophys. 1970;13:937–68.
[54] Dickinson WR, Beard LS, Brakenridge GR, Erjavec JL, Ferguson RC, Inman KF, et al. Provenance of North American Phanerozoic sandstones in relation to tectonic setting. GSA. 1983;94:222–35.
[55] Pettijohn FJ, Potter PE, Siever R. Sand and Sandstone. New York: Springer-Verlag; 1972. p. 618.
[56] Herron MM. Geochemical classification of terrigenous sands and shales from core or log data. J Sediment Petrology. 1988;58:820–29.
[57] Bhatia MR, Crook KAW. Trace element characteristics of graywackes and tectonic setting discrimination of sedimentary basins. Contributions mineralogy petrology. 1986;92(2):181–93.
[58] McLennan SM, Hemming S, McDaniel DK, Hanson GN. Geochemical approaches to sedimentation, provenance and tectonics. Processes Controlling the Composition of Clastic Sediments; 1993.
[59] Taylor SR, McLennan SM. Composition and evolution of the continental crust: rare earth element evidence from sedimentary rocks [and discussion]. Philos Trans R Soc A: Mathematical, Phys Eng Sci. 1981;301:399–99.
[60] Sun SS, McDonough WF. Chemical and isotopic systematics of oceanic basalts: implications for mantle composition and processes. Geol Society, Lond Spec Publ. 1989;42:313–45.
[61] McLennan SM. Rare-earth elements in sedimentary rocks: influence of provenance and sedimentary processes. Geochem Mineralogy Rare Earth Elem. 1989;21:169–200.
[62] Wang ZG, Yu XY, Zhao ZH. Rare Earth Element Geochemistry. Beijing: Science Press (in chinese); 1989.
[63] Armstrong-Altrin JS, Lee YI, Verma SP, Ramasamy S. Geochemistry of sandstones from the Upper Miocene Kudankulam Formation, southern India: implications for provenance, weathering, and tectonic setting. J Sediment Res. 2004;74:285–97.
[64] Nesbitt HW, Young GM. Prediction of some weathering trends of plutonic and volcanic rocks based on thermodynamic and kinetic considerations. Geochim Cosmochim Acta. 1984;48:1523–34.
[65] Fedo CM, Nesbitt HW, Young GM. Unraveling the effects of potassium metasomatism in sedimentary rocks and paleosols, with implications for paleoweathering conditions and provenance. Geology. 1995;23:921–24.
[66] Monghaddam SP, Salehi MA, Jafarzadeh M, Zohdi A. Provenance, palaeoweathering and tectonic setting of the ediacaran bayandor formation in nw iran: implications for the northern gondwana continental margin during the late neoproterozoic. J Afr Earth Sci. 2020;161:103670.1–103670.16.
[67] Scarciglia F, Le Pera E, Critelli S. The onset of sedimentary cycle in a mid-latitude upland environment: weathering, pedogenesis and geomorphic processes on plutonic rocks (Sila Massif, Calabria). In: Arribas J, Critelli S, Johnsson M, editors.

Sedimentary Provenance: Petrographic and Geochemical Perspectives. Geological Society of America Special Paper. vol. 420; 2007. p. 149–66.
[68] Salehi MA, Mazroei Sebdani Z, Pakzad HR, Bahrami A, Fürsich FT, Heubeck C. Provenance and palaeogeography of uppermost Triassic and Lower Cretaceous terrigenous rocks of central Iran: reflection of the Cimmerian events. Neues Jahrb Geol Palaontol Abh. 2018;288(1):49–77.
[69] Van de Kamp PC, Leake BE, Bernard E. Petrography and geochemistry of feldspathic and mafic sediments of the northeastern Pacific margin. Earth Environ Sci Trans R Soc Edinb. 1985;76(4):411–49.
[70] Barshad I. The effect of a variation in precipitation on the nature of clay mineral formation in soils from acid and basic igneous rocks. Proceedings International Clay Conference. Jerusalem: 1966. p. 167–73.
[71] Baker RJ. Uranium minerals and their relevance to long term storage of nuclearfuels. Coord Chem Rev. 2014;266–267:123–36.
[72] Boekhout F, Gerard M, Kanzari A, Michel A, Dejeant A, Galoisy L, et al. Uranium migration and retention during weathering of a granitic wasterock pile. Appl Geochem. 2015;58:123–35.
[73] Garcia D, Ravenne C, Maréchal B, Moutte J. Geochemical variability induced by entrainment sorting: Quantified signals for provenance analysis. Sediment Geol. 2004;171(1–4): 113–28.
[74] Armstrong-Altrin JS. Provenance of sands from Cazones, Acapulco, and Bahía Kino beaches, Mexico. Revista Mexicana de Ciencias Geológicas. 2009;26(3):764–82.
[75] Etemad-Saeed N, Hosseini-Barzi M, Armstrong-Altrin JS. Petrography and geochemistry of clastic sedimentary rocks as evidences for provenance of the lower cambrian lalun formation, posht-e-badam block, central iran. J Afr Earth ences. 2011;61(2):142–59.
[76] Zaid SM. Geochemistry of sandstones from the pliocene gabir formation, north marsa alam, red sea, egypt: Implication for provenance, weathering and tectonic setting. J Afr Earth Sci. 2015;102(feb):1–17.
[77] Ahmad I, Chandra R. Geochemistry of loess-paleosol sediments of Kashmir Valley, India: provenance and weathering. J Asian Earth Sci. 2013;66:73–89.
[78] Song MS. sedimentary environment geochemistry in the shasi section of southern ramp,dongying depression. Miner Pet. 2005;25(1):67–73 (in Chinese with English abstract).
[79] Xu H, Liu YQ, Liu YX, Kuang HW. Stratigraphy, sedimentology and tectonic background of basin evolution of the Late Jurassic-Early Cretaceous Tuchengzi Formation in Yinshan-Yanshan, North China. Earth Sci Front. 2011;18(4):88–106 (in Chinese with English abstract).
[80] Maynard JB, Valloni R, Yu HS. Composition of modern deep-sea sands from arc-related basins. Geol Soci Lond Spec Publ. 1982;10(1):551–61.
[81] Floyd PA, Leveridge BE. Tectonic environment of the devonian gramscatho basin, south cornwall: Framework mode and geochemical evidence from turbidite sandstones. J Geol Soc Lond. 1987;144(4):531–42.
[82] Floyd PA, Winchester JA, Park RG. Geochemistry and tectonic setting of lewisian clastic metasediments from the early proterozoic loch maree group of gairloch, nw scotland. Precambrian Res. 1989;45(1–3):203–14.
[83] Gu XX, Liu JM, Zheng MH, Tang JX, Qi L. Provenance and tectonic setting of the proterozoic turbidites in Hunan, south China: Geochemical evidence. J Sediment Res. 2002;72(3):393–407.
[84] Condie KC. Chemical composition and evolution of the upper continental crust: Contrasting results from surface samples and shales. Chem Geol. 1993;104(1–4):37.
[85] Roser BP, Korsch RJ. Determination of tectonic setting of sandstone-mudstone suites using SiO_2 content and K_2O/Na_2O ratio. J Geol. 1986;94(5):635–50.
[86] Mader D, Neubauer F. Provenance of Palaeozoic sandstones from the Carnic Alps (Austria): Petrographic and geochemical indicators. Int J Earth Sci. 2004;93(2):262–81.
[87] Guo QQ, Xiao WJ, Windley BF, Mao QG, Han CM, Qu JF, et al. Provenance and tectonic settings of Permian turbidites from the Beishan Mountains, NW China: Implications for the Late Paleozoic accretionary tectonics of the southern Altaids. J Asian Earth Sci. 2012;49:54–68.
[88] Bhatia MR. Rare earth element geochemistry of Australian Paleozoic graywackes and mudrocks: Provenance and tectonic control. Sediment Geol. 1985;45(1–2):97–113.
[89] Bhatia MR. Plate tectonics and geochemical composition of sandstones. J Geol. 1983;91(6):611–27.
[90] Maynard JB, Valloni R, Yu HS. Composition of modern deep-sea sands from arc-related basins. Geol Society, Lond Spec Publ. 1982;10(1):551–61.
[91] Xiao LL, Liu FL. Precambrian metamorphic history of the metamorphic complexes in the Trans-North China Orogen. North China Craton Acta Pet Sin. 2015;31:3012–44.
[92] Liu F, Zhang J, Liu C. Archean to paleoproterozoic evolution of the north china craton: Preface. Precambrian Res. 2017;303:1–9.
[93] Wan Y, Xu Z, Dong C, Nutman A, Ma M, Xie H. Episodic paleoproterozoic (2.45, 1.95 and 1.85 Ga) mafic magmatism and associated high temperature metamorphism in the Daqingshan area, north china craton: Shrimp zircon U–Pb dating and whole-rock geochemistry. Precambrian Res. 2013;224:71–93.
[94] Peng P, Bleeker W, Ernst RE, Söderlund U, McNicoll V. U–Pb baddeleyite ages, distribution and geochemistry of 925 Ma mafic dykes and 900 Ma sills in the North China craton: Evidence for a Neoproterozoic mantle plume. Lithos. 2011a;127:210–21.
[95] Peng P, Zhai MG, Li QL, Wu FY, Hou QL, Li Z, et al. Neoproterozoic (~900 Ma) Sariwon sills in North Korea: geochronology, geochemistry and implications for the evolution of the south-eastern margin of the North China Craton. Gondwana Res. 2011b;20:243–54.
[96] Zhang SH, Zhao Y, Ye H, Liu JM, Hu ZC. Origin and evolution of the Bainaimiao arc belt: Implications for crustal growth in the southern Central Asian orogenic belt. Geol Soc Am Bull. 2014;126:1275–300.
[97] Zhang SH, Zhao Y, Song B, Hu JM, Liu SW, Yang YH, et al. Contrasting Late Carboniferous and Late Permian-Middle Triassic intrusive suites fromthe northern margin of the North China Craton: Geochronology, petrogenesis and tectonic implications. Geol Soc Am Bull. 2009;121:181–200.
[98] Zhang SH, Zhao Y, Liu JM, Hu ZC. Different sources involved in generation of continental arc volcanism: The carboniferous-permian volcanic rocks in the northern margin of the north china block. Lithos. 2016;240–243:382–401.